





Tunable transverse optical force via nonreciprocity

Mengkai Che ¹, Huimin Zhu,² Xiaoxuan Shi ¹, Yaxin Li ¹, Xiao Li ³, Lei Zhang,^{2,4,*} and Jun Chen^{1,4,†}

¹State Key Laboratory of Quantum Optics and Quantum Optics Devices,
Institute of Theoretical Physics, Shanxi University, Taiyuan 030006, China

²State Key Laboratory of Quantum Optics and Quantum Optics Devices,
Institute of Laser Spectroscopy, Shanxi University, Taiyuan 030006, China

³Department of Physics, The Hong Kong University of Science and Technology, Hong Kong, China

⁴Collaborative Innovation Center of Extreme Optics, Shanxi University, Taiyuan 030006, China



(Received 4 December 2023; revised 18 February 2024; accepted 8 April 2024; published 24 April 2024)

The transverse optical force adds an extra degree of freedom for optical manipulation. In this paper, based on the full wave simulation, we find that an achiral sphere can experience a transverse optical force in the field of a circularly polarized or linearly diagonally polarized electric dipole source in the vicinity of a doped InSb substrate. When the dipole is circularly polarized, the transverse force results from the asymmetrical distribution of the excited surface waves. However, when the dipole is linearly diagonally polarized, the transverse force stems from the combined effect of the surface waves and asymmetrical propagating waves. More importantly, the magnitude and direction of the transverse force can be adjusted by applying a magnetic field parallel to the InSb substrate, due to the generated additional nonreciprocity. Our paper expands the scope of transverse optical force by nonreciprocity.

DOI: [10.1103/PhysRevA.109.043527](https://doi.org/10.1103/PhysRevA.109.043527)

I. INTRODUCTION

Recently, significant research interest has emerged in the transverse optical force. This force typically emerges from the breaking of some form of symmetry. Examples include inherent asymmetry in chiral material or chiral structure systems [1–3], broken symmetry in geometry [4,5], the breaking of electric-magnetic symmetry [6], scattering asymmetry induced by spin-orbit coupling [7–9], directional Belinfante spin momentum or transverse spin angular momentum of the incident field [10–12], and others [13–16].

An evanescent wave is a typical optical field that generates transverse optical force. It can be generated through total internal reflection at the interface between two media [12,17–21]. One notable advantage of this mechanism is its ability to produce evanescent waves with various polarization states [10,12,19–22]. It has been found that an evanescent wave with circular or diagonal linear polarization can induce a transverse optical force on an achiral spherical particle, where both the incident field and the illuminated particle exhibit no apparent left-right asymmetry [10,12]. However, the amplitude of the transverse optical force generated by this evanescent wave is relatively small [12]. Surface-plasmon polaritons (SPPs), propagating at the interface between dielectric and metallic materials, are also a type of evanescent wave. These surface waves can be generated using configurations such as the Kretschmann and Otto configurations [23]. The optical force within this field can be significantly enhanced due to its high

local energy density [23,24]. However, SPPs are typically limited to the transverse magnetic polarization mode. This limitation arises from the requirement of continuity in electromagnetic boundary conditions at the interface between the two media [24,25]. As a result, the generation of a transverse optical force from the reciprocal SPPs is forbidden [12]. Thus, designing a system that combines enhanced optical fields with a flexible tuning mechanism to generate a transverse optical force becomes important.

In this paper, as illustrated in Fig. 1(a), we consider a physical system comprising an electric dipole source near a doped InSb substrate and a manipulated particle. The dipole source positioned above the substrate provides the manipulated particle with an optical field containing rich polarization information [11,29,30] and high local energy density [23–25], among other characteristics [31–33]. This radiation source could be an optical probe of a scanning near-field optical microscope [34,35], a small illuminated particle in the Rayleigh limit [36,37], or something similar [2,38,39], with a diverse wave-vector distribution [37,40]. The dipole sources can simultaneously generate propagating and evanescent waves. When the dipole source is in close proximity to a substrate, it can excite the surface waves. Due to the conservation of momentum, the surface waves exhibit the same asymmetry as the evanescent components of the dipole source [37,40–44]. Furthermore, the surface waves on the InSb substrate can become nonreciprocal [asymmetric dispersion $\omega(\mathbf{k}) \neq \omega(-\mathbf{k})$] and tuned when a magnetic field is applied parallel to its surface (along the y direction). To generate surface waves on the doped InSb substrate and ensure that these waves respond well to a magnetic field, we use a dipole source with a radiation wavelength of 50 μm . This parameter setting aids

*zhanglei@sxu.edu.cn

†chenjun@sxu.edu.cn

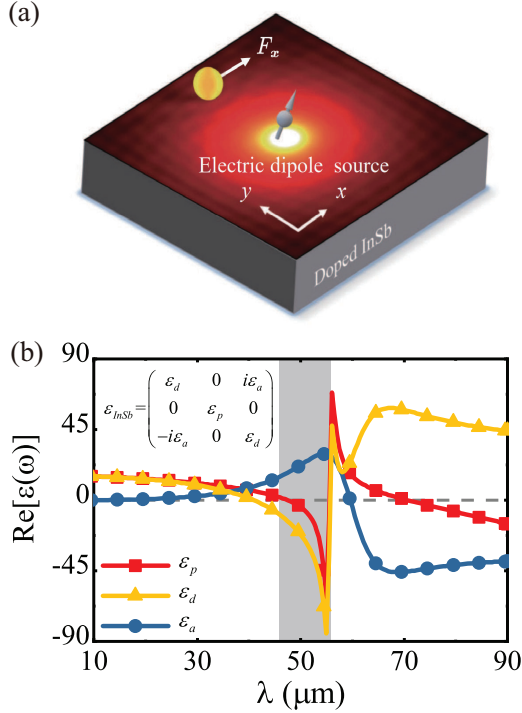


FIG. 1. (a) Schematic plot illustrating a manipulated polystyrene sphere in the optical field of an electric dipole source near a doped InSb [26,27] substrate. (b) The real part of InSb's dielectric tensor components vs the wavelength at a magnetic field of $B = 1$ T. Refer to the inset for the specific form of the dielectric tensor [28]. The shaded area indicates the approximate locations of SPhPs.

in achieving combined modulation of various mechanisms on the transverse optical force. The excited surface waves in this instance are mainly the surface phonon polaritons (SPhPs) [45], as shown in Fig. 1(b). SPhPs result from the coupling between electromagnetic waves and optical phonons of polar materials. They are active in the midinfrared and share similar characteristics with SPPs, such as propagation along a boundary, and high field density at the surface, among others [45,46].

We explored the transverse optical force under the interplay of multiple mechanisms based on full wave simulations. It is found that, in the absence of magnetic field, the propagating component of a circularly polarized electric dipole radiation [$\mathbf{p} = (1, 0, i)$] is symmetrical in the x direction while it exhibits an asymmetric spectrum in its evanescent component. When it is placed in proximity to the InSb substrate, the surface waves are excited by the evanescent component. Then the particle on the y axis will experience transverse optical force due to asymmetric surface waves. In the case of a linearly diagonally polarized electric dipole source [$\mathbf{p} = (1, 0, 1)$], the propagating waves are asymmetrical in the x direction, generating the transverse optical force on the particle placed on the y axis. Although the surface wave does not display evident left-right asymmetry, the oblique linear polarization properties of the total field along the y axis will still generate a transverse optical force on the particle. This total field primarily consists of the SPhPs excited by the p -polarized component of the electric dipole source,

as well as the propagating wave from both the p - and s -polarized components of the electric dipole source. Hence, the transverse optical force on the particle results from the competition between these two mechanisms. Additionally, the magnetic field applied in the InSb substrate introduces another nonreciprocal [46–49] competition mechanism. We discover that the magnitude and sign of the transverse optical force can be further controlled by the magnetic field in both the circularly polarized and linearly diagonally polarized electric dipole cases.

II. TRANSVERSE OPTICAL FORCE WITHOUT MAGNETIC FIELD

Before investigating the transverse optical force exerted on the manipulated particle in Fig. 1(a), we first analytically analyze the optical field generated by an electric dipole in free space. For an electric dipole $\mathbf{p} = (p_x, p_y, p_z)$ placed at $\mathbf{h} = (0, 0, z_0)$, the radiated electric field \mathbf{E} can be expressed using the angular spectrum as follows [25,29,42,50]:

$$\mathbf{E}(x, y, z) = \iint_{-\infty}^{\infty} \mathbf{E}(k_x, k_y; z_0) e^{i(k_x x + k_y y + k_z |z - z_0|)} dk_x dk_y, \quad (1)$$

in which the time dependence $e^{-i\omega t}$ has been assumed and omitted for simplicity. When projected onto the s - and p -polarized basis vectors ($\hat{\mathbf{e}}_s$ and $\hat{\mathbf{e}}_p^\pm$), the angular spectrum of the electric field can be written as the sum of the s - and p -polarized components [37]:

$$\mathbf{E}(k_x, k_y; z_0) = \frac{ik^2}{8\pi^2 \epsilon_0 k_z} [(\hat{\mathbf{e}}_s \cdot \mathbf{p}) \hat{\mathbf{e}}_s + (\hat{\mathbf{e}}_p^\pm \cdot \mathbf{p}) \hat{\mathbf{e}}_p^\pm], \quad (2)$$

where $+$ and $-$ symbols in $\hat{\mathbf{e}}_p^\pm$ indicate the fields calculated above and below $z = z_0$, respectively. $\hat{\mathbf{e}}_s$ and $\hat{\mathbf{e}}_p^\pm$ are defined as

$$\hat{\mathbf{e}}_s(k_x, k_y) = \left(-\frac{k_y}{k_\rho}, \frac{k_x}{k_\rho}, 0 \right),$$

$$\hat{\mathbf{e}}_p^\pm(k_x, k_y) = \left(\pm \frac{k_x k_z}{k k_\rho}, \pm \frac{k_y k_z}{k k_\rho}, -\frac{k_\rho}{k} \right). \quad (3)$$

Here, k represents the wave number in the background medium, and $k_\rho = \sqrt{k_x^2 + k_y^2}$ satisfies $k_\rho^2 + k_z^2 = k^2$.

The angular spectrum of electric dipole radiation, as described in Eq. (2), offers direct insights into the directionality of both evanescent and propagating components. The p -polarized components of the angular spectrum for a circularly polarized and a linearly diagonally polarized electric dipole along k_x (assuming $k_y = 0$) are plotted in Figs. 2(a) and 2(b), respectively. As shown in Fig. 2(a), a circularly polarized dipole [$\mathbf{p} = (1, 0, i)$] in the xz plane shows symmetry for the propagating component ($|k_x| < k$, as also shown in the inset for dipole radiation in free space) and asymmetry for the evanescent part ($|k_x| > k$). Conversely, Fig. 2(b) presents a linearly diagonally polarized dipole [$\mathbf{p} = (1, 0, 1)$] in the xz plane, which displays asymmetry for the propagating component ($|k_x| < k$, as also depicted in the inset) and symmetry for the evanescent part ($|k_x| > k$). In addition, Eqs. (2) and (3) reveal that for both polarization states of the dipole source considered, the

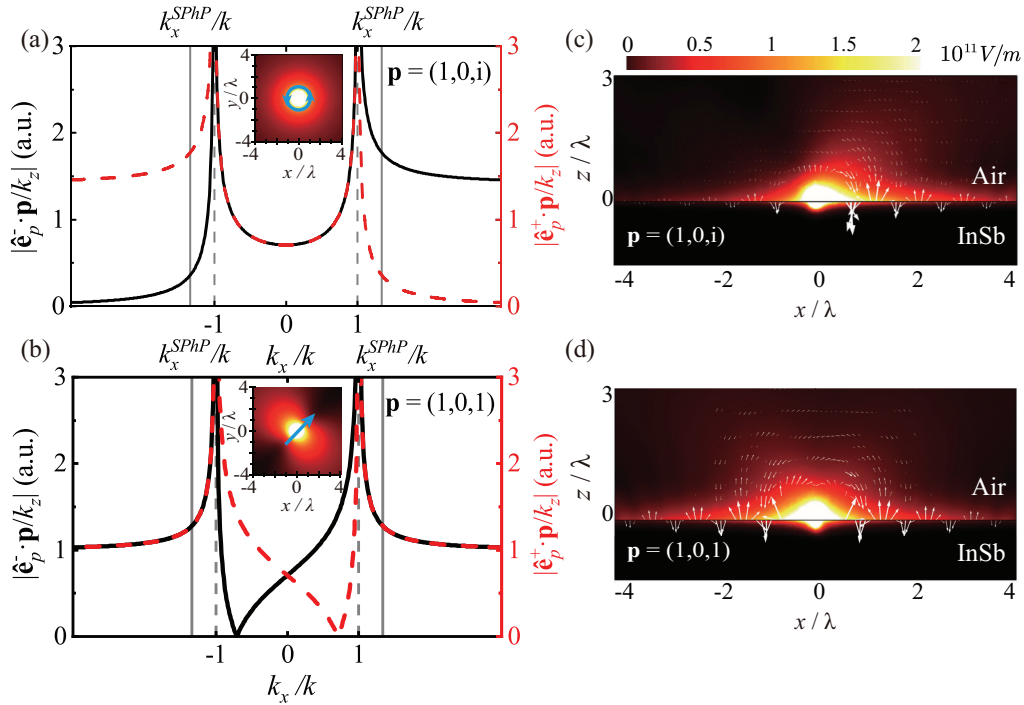


FIG. 2. The absolute values of the angular spectrum for the p -polarized component along k_x ($k_y = 0$) are displayed for an electric dipole source with circular polarization (a) and diagonal linear polarization (b). The insets illustrate the amplitude of the electric field for the dipole source radiating in free space. (c, d) Electric field induced by an electric dipole source in the presence of a doped InSb substrate with the permittivity described by the Drude model [26,28]. The dipole source is positioned at $z_0 = 0.5 \mu\text{m}$ above the substrate surface. The source displays circular and diagonal linear polarization in (c) and (d), respectively. The color map and white arrows signify the amplitude and direction of the electric field. The dipole sources used in (c) and (d) and the insets in (a) and (b) have a radiation wavelength of $50 \mu\text{m}$, with a dipole strength of $2.544 \times 10^{-14} \text{ C m}$. The color bars for (c) and (d) and for the insets in (a) and (b) are unified, as shown in (c).

s -polarized component of the angular spectrum always maintains symmetry about k_x for both propagating and evanescent components [37]. Hence, the directionality of the electric dipole's radiation is determined exclusively by the p -polarized component.

The evanescent component ($|k_x| > k$) of the p -polarized angular spectrum can play a crucial role [37,40–42] when the dipole source is near the doped InSb substrate. When we consider the midinfrared wavelengths, because of momentum conservation, this evanescent component matches the parallel wave vector of the substrate-supported surface phonon, efficiently exciting the SPhPs [37,42,45,46]. These SPhPs demonstrate the same asymmetry as the evanescent component of the dipole source. Figures 2(c) and 2(d) display the electric field induced by an electric dipole source in the presence of the doped InSb substrate, as calculated by the numerical solver COMSOL MULTIPHYSICS. The color map denotes the amplitude of the electric field, while the white arrows indicate its direction. We can clearly see that the SPhPs are excited. When considering a circularly polarized dipole source, the excited SPhPs show asymmetry along the x axis [see Fig. 2(c)]. This asymmetry arises from the evanescent component of the dipole source, which is asymmetric along k_x [refer to the solid black line in Fig. 2(a)]. However, when using a linearly diagonally polarized dipole source near the InSb surface, the excited SPhPs exhibit symmetry as the evanescent component of the source [see Fig. 2(d) and the solid black line in Fig. 2(b)].

In addition to the SPhPs above the InSb substrate, there are also the propagating waves from the dipole source. Hence, when a manipulated particle is positioned above the substrate, the resulting optical force on the particle is affected by the source's propagating waves and the excited surface waves. In the following, we mainly concentrate on the transverse optical force exerted on the manipulated particle when there is no applied magnetic field as shown in Fig. 1(a). The optical force is calculated by integrating the Maxwell stress tensor along a closed boundary around the particle [51,52], which is normalized by the power radiated by the dipole source ($P_{\text{rad}} = \omega^4 |\mathbf{p}|^2 / 12\pi \epsilon_0 c^3$ [11,36,50,53]). The total optical fields are computed by the full wave simulation via COMSOL MULTIPHYSICS.

We first consider a scenario where the electric dipole source is circularly polarized [$\mathbf{p} = (1, 0, i)$]. It is found that an isotropic polystyrene sphere on the y axis ($x = 0, z = 15 \mu\text{m}$) experiences a nonzero transverse optical force (F_x) as shown in Fig. 3(e). This is due to the excited asymmetrical SPhPs as presented in Fig. 2(c). The asymmetrical distribution of the optical field can also be found in the xy plane in Fig. 3(a). Since the optical field is primarily distributed in the $+x$ direction, its induced transverse optical force on the polystyrene sphere is positive. As expected, the transverse optical force decreases when the polystyrene sphere moves away from the electric dipole source due to its decaying property.

Interestingly, we discover that when the electric dipole source becomes linearly diagonally polarized [$\mathbf{p} = (1, 0, 1)$],

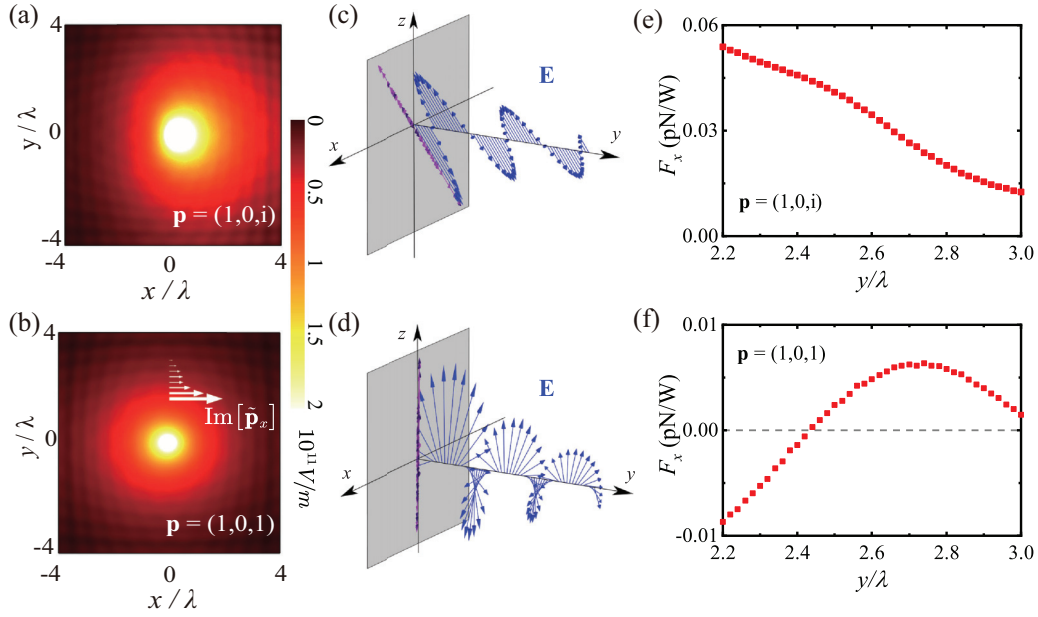


FIG. 3. Transverse optical force exerted on a polystyrene sphere [see the system depicted in Fig. 1(a)]. (a), (b) Electric field, induced by an electric dipole source in the presence of a doped InSb substrate, plotted on the xy plane with $z = 15 \mu\text{m}$. The dipole source is positioned at $z_0 = 0.5 \mu\text{m}$ above the substrate surface, with a radiation wavelength of $50 \mu\text{m}$ and a strength of $2.544 \times 10^{-14} \text{ C m}$. The source carries circular and diagonal linear polarization in (a) and (b), respectively. The color map denotes the electric field's amplitude. The white arrows in (b) represent the x component of the complex Poynting vector's imaginary part within the considered region on the y axis ($x = 0, z = 15 \mu\text{m}$). (c), (d) Instantaneous distribution of the real electric field propagating along the y axis ($x = 0$) in the case of an electric dipole $\mathbf{p} = (1, 0, 1)$ without and with a doped InSb substrate. The purple arrows represent the projection of the electric field on the xz plane. (e), (f) Transverse optical force when a polystyrene sphere is located on the y axis ($x = 0, z = 15 \mu\text{m}$) in the optical fields of (a) and (b). The polystyrene sphere has a permittivity of 2.52 and a radius of $10 \mu\text{m}$.

the same polystyrene sphere positioned on the y axis can experience either a positive or negative transverse force depending on its positions. The numerical results are shown in Fig. 3(f). Contrary to the results from the circularly polarized dipole source, the transverse optical force initially is negative and gradually shifts to positive values along y axis. This can be understood as follows. As illustrated in Figs. 2(b) and 2(d), only the propagating component of the electric dipole radiation along the x axis is asymmetrical, and it tends to propagate in the $-x$ direction at the region $z > z_0$. This raises a question: why can the optical force take positive values? The asymmetry of the amplitude of the electric dipole radiation's propagation component along the x axis is critical for generating transverse optical forces. However, its polarization state is also important. As shown in Fig. 3(c), the propagation component of the electric dipole $\mathbf{p} = (1, 0, 1)$ remains linearly diagonally polarized in the xz plane. In the presence of the doped InSb substrate, the total field decays in the z direction with an oblique linear polarization characteristic [see Fig. 3(d)]. In contrast, the total field has an imaginary longitudinal y component, which results in rotations of the electric field in the propagation yz plane. This generate a nonzero transverse spin stemming from the complex Poynting vector's imaginary part along the x axis, $\text{Im}[\tilde{\mathbf{p}}_x]$ [see the white arrows in Fig. 3(b)], leading to the generation of a transverse optical force [10,12]. Therefore, as depicted by the red squares in Fig. 3(f), the transverse optical force results from the competition between the two mechanisms. Specifically, the asymmetry of the magnitude of the propagating component generates a $-x$ direction

transverse optical force on the polystyrene sphere placed on the y axis. Meanwhile, the complex Poynting vector's imaginary part of the total field induces an $+x$ direction transverse optical force. Consequently, two transverse optical force mechanisms compete with each other. When the polystyrene sphere is near the electric dipole source, the asymmetry of the dipole radiation's propagating component is dominant, resulting in a negative transverse force on the sphere. As the sphere moves away from the electric dipole source, the impact of the propagating component reduces. The transverse optical force mechanism, caused by the oblique linearly polarized total field, becomes increasingly dominant. Consequently, the force exerted on the polystyrene sphere turns positive. Finally, as the distance between the sphere and the electric dipole source further increases, both the propagating component and the surface waves weaken, leading to a reduction in the optical force.

III. TUNING OF TRANSVERSE OPTICAL FORCE VIA MAGNETIC FIELD

Besides enhancing the optical field, another benefit of using a doped InSb [28,54–56] substrate is its effective response to applied magnetic fields. As illustrated in Fig. 4(a), the InSb substrate supports reciprocal SPhPs along the x axis when there is no magnetic field [refer to the solid orange line in Fig. 4(a)]. When a magnetic field is applied along the y axis (using the Voigt configuration), due to the breaking of time-reversal symmetry, the SPhPs becomes nonreciprocal as

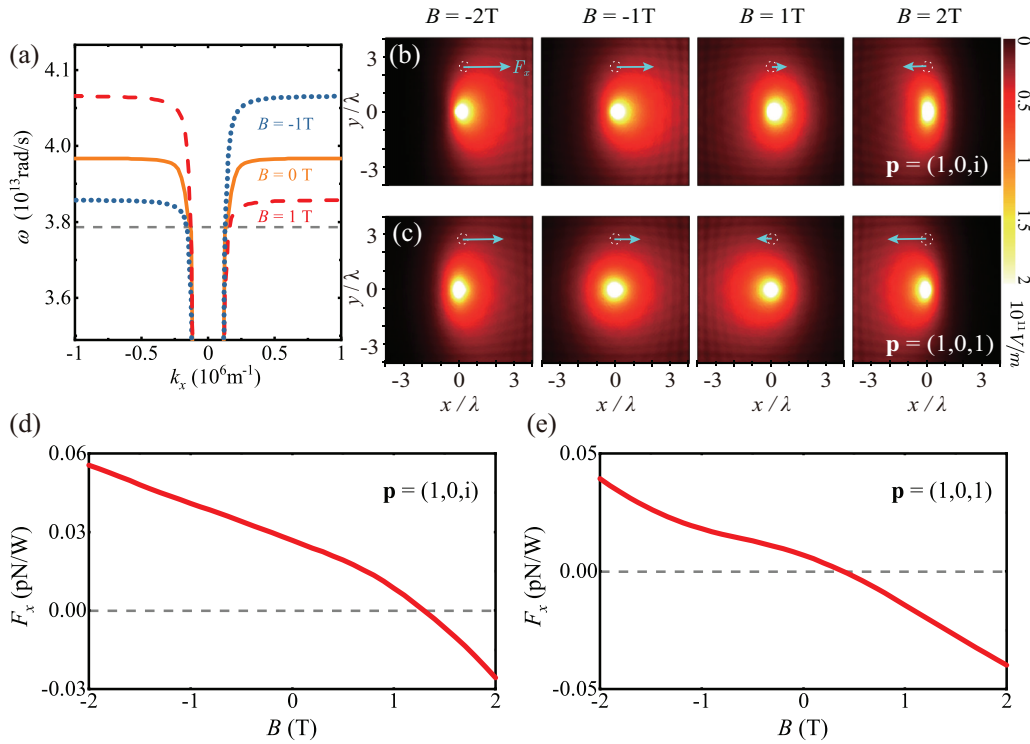


FIG. 4. (a) The dispersion of SPhPs vs k_x with $k_y = 0$ supported by the doped InSb substrate. The solid orange line depicts the symmetric dispersion of SPhPs with zero magnetic field, while the dashed red and dotted blue lines show the asymmetric dispersion of SPhPs with magnetic fields of $B = 1$ and -1 T, respectively. The horizontal gray dashed line corresponds to the frequency used in this paper. (b, c) The electric field generated by an electric dipole source in the presence of an InSb substrate plotted on the xy plane at $z = 15$ μm when a magnetic field of various values is applied along the y axis (the Voigt configuration). The dipole source is situated 0.5 μm above the substrate surface, with a radiation wavelength of 50 μm and a strength of 2.544×10^{-14} C m. The electric dipole source carries circular and diagonal linear polarization in (b) and (c), respectively. The color map represents the amplitude of the electric field. (d, e) Transverse optical forces vs the magnetic field. The polystyrene sphere with a permittivity of 2.52 and a radius of 10 μm is located at $(x/\lambda, y/\lambda, z/\lambda) = (0, 2.7, 0.3)$, as shown by the white dashed circles in (b) and (c).

shown by the dashed red and dotted blue lines in Fig. 4(a). This nonreciprocity, induced by the magnetic field, introduces another mechanism to further tune the transverse optical force.

In the case of a circularly polarized electric dipole source, the transverse optical force arises from the asymmetric excitation of SPhPs, according to the discussion in the above section. In the absence of a magnetic field, the amplitude of SPhPs propagating in the $+x$ direction is larger [see Fig. 3(a)]. Therefore the polystyrene sphere on the y axis experiences a transverse optical force pointing in the $+x$ direction [see Fig. 3(e)]. When a magnetic field along the $-y$ direction is applied, the linear momentum of SPhPs propagating in the $+x$ direction is larger than that of SPhPs propagating in the $-x$ direction [see Fig. 4(a)]. Thus, both the electric dipole source and the magnetic field modulate the asymmetric propagation of SPhPs, enhancing the optical field propagating in the $+x$ direction [see the first two columns of Fig. 4(b)]. As the magnitude of the magnetic field along the $-y$ direction increases, the asymmetric propagation of the optical field along the $+x$ direction also increases, leading to an increased transverse optical force in the $+x$ direction [see Figs. 4(b) and 4(d)]. The direction and length of the turquoise arrows in Fig. 4(b) represent the direction and relative magnitude of the force on the polystyrene sphere at that location. However, when a magnetic field along the $+y$ direction is applied, the magnetic field's

control of the SPhPs dispersion and the asymmetric excitation of SPhPs by the electric dipole source are opposite. The resultant competition between these two mechanisms leads to a decreased positive transverse optical force. As the strength of the magnetic field continues to increase, the direction of the transverse optical force eventually reverses, as shown in the last two columns of Figs. 4(b) and 4(d). It is worth mentioning that the transverse optical forces are asymmetric with respect to B , i.e., $F_x(B) \neq F_x(-B)$. Therefore, the doped InSb substrate can operate as a transverse optical force rectifier when the dipole is circularly polarized.

In the case of a linearly diagonally polarized electric dipole source, the magnitude and direction of the transverse optical force are now determined by three mechanisms. These mechanisms include the asymmetry of the source's propagating component, the complex Poynting vector's imaginary part of the total field, and the nonreciprocal dispersion of SPhPs due to the magnetic field. For instance, in the absence of a magnetic field, when the polystyrene sphere is located on the y axis [coordinates are $(x/\lambda, y/\lambda, z/\lambda) = (0, 2.7, 0.3)$], the transverse force resulting from the source's propagating component asymmetry is directed in the $-x$ direction. In contrast, the transverse force stemming from the complex Poynting vector's imaginary part of the total field points in the $+x$ direction. This results in a net transverse force toward

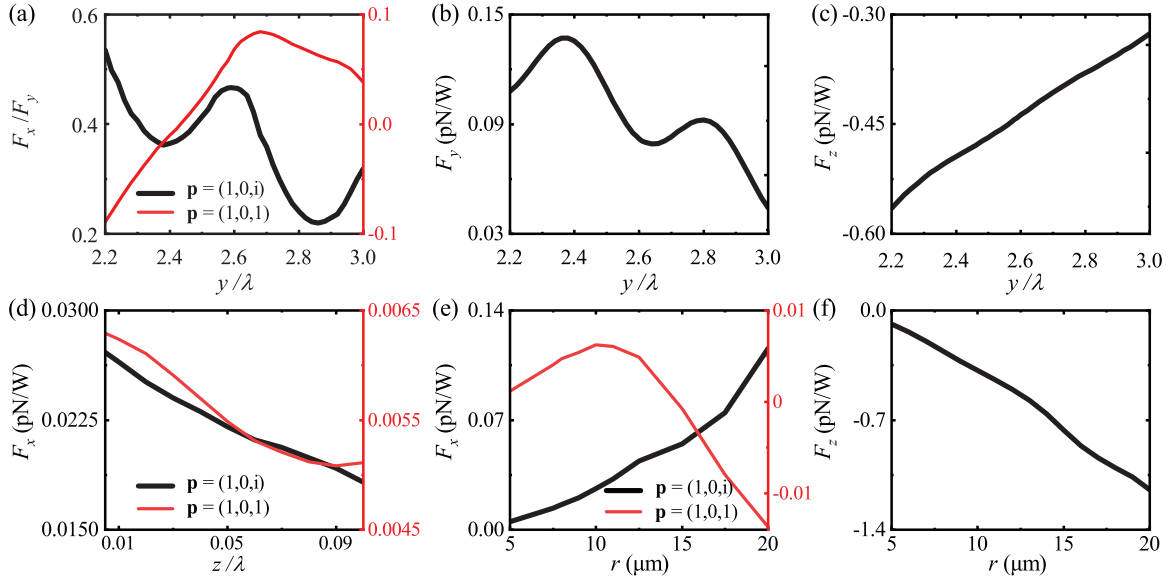


FIG. 5. (a) The ratio of the transverse force to the longitudinal force (F_x/F_y) vs the polystyrene sphere's position on the y axis ($x = 0, z = 15 \mu\text{m}$) for both circularly polarized and linearly diagonally polarized dipole source cases. (b) The longitudinal force F_y and (c) the optical force F_z perpendicular to the substrate, exerted on a polystyrene sphere vs the spheres' position on the y axis ($x = 0, z = 15 \mu\text{m}$). (d) The transverse optical force exerted on a polystyrene sphere located at $(x/\lambda, y/\lambda, z/\lambda) = (0, 2.7, 0.3)$ vs the distance between the dipole source and substrate surface. (e, f) F_x and F_z exerted on a polystyrene sphere located at $(x/\lambda, y/\lambda) = (0, 2.7)$ vs the spheres' radius. The polystyrene sphere in (e) and (f) is positioned $5 \mu\text{m}$ away from the $z = 0$ plane at their base. The polystyrene sphere (with a permittivity of 2.52) has a radius of $10 \mu\text{m}$ in (a)–(d). The dipole source, with a radiation wavelength of $50 \mu\text{m}$, is positioned at $z_0 = 0.5 \mu\text{m}$ above the substrate surface except in (d). In (a), (d), and (e), the results in the cases of circularly polarized and linearly diagonally polarized dipole sources are presented in the left and right vertical axes, respectively.

the $+x$ direction, as shown in Figs. 3(f) and 4(e). When a magnetic field is applied, the intensity of the optical field and, consequently, the transverse force, is affected. For instance, a magnetic field in the $-y$ direction intensifies the optical field propagating in the $+x$ direction and increases the transverse force towards the $+x$ direction [see Figs. 4(c) and 4(e)]. However, a magnetic field along the $+y$ direction increases the optical field propagating in the $-x$ direction, causing the transverse force in the reverse direction. Comparing Figs. 4(d) and 4(e), the transverse optical forces are less asymmetric with respect to B when the dipole is linearly diagonally polarized.

IV. DISCUSSION ON THE ENHANCEMENT OF TRANSVERSE OPTICAL FORCE

In the above, a polystyrene sphere is chosen to effectively clarify the physical mechanism of transverse optical force. Although the ratio of transverse to longitudinal force (F_x/F_y) varies between 0.2 and 0.6 in the case of a circularly polarized electric dipole source, it falls within a range of 0.1 for a linearly diagonally polarized source [see Fig. 5(a)]. This indicates that the transverse optical force can be comparable to the longitudinal optical force. However, the magnitudes of both the transverse [Figs. 3(e) and 3(f)] and longitudinal forces [same for both polarized dipole sources, see Fig. 5(b)] exerted on the polystyrene sphere are relatively small due to the minor difference in permittivity between polystyrene and background air. Moreover, the optical force F_z exerted on the polystyrene sphere in the direction perpendicular to the substrate is negative [same for both polarized dipole sources, as

shown in Fig. 5(c)]. This means it points towards the substrate, aligning with the direction of gravitational force. This causes the polystyrene sphere to position extremely close to the substrate surface, resulting in a larger van der Waals force. These may make the polystyrene sphere difficult to manipulate. To enhance the transverse optical force for easier manipulation, we further investigate the effects of various parameters, such as the material and radius of the sphere, as well as the distance between the dipole source and substrate, etc.

First, we examine the effect of the dipole source-substrate distance on the transverse optical force. As shown in Fig. 5(d), the transverse force decreases as the dipole source moves away from the substrate, regardless of the type of polarization of the dipole source. This decrease is due to the decay of evanescent components that can effectively excite SPPs or SPhPs before reaching the substrate, reducing the coupling efficiency between source photons and surface plasmons or phonons. However, it should be noted that a closer distance between the dipole source and substrate is not necessarily better. The intrinsic loss mechanisms in nonradiative processes caused by interband transitions, electron scattering loss, and electron-hole excitation can also lower the coupling efficiency [2]. Taking into account the calculation accuracy and efficiency, we set the dipole source at $z_0 = 0.5 \mu\text{m}$ ($z_0/\lambda = 0.01$) above the substrate surface.

Next, we investigate the effect of the radius on the transverse optical force. As seen in Fig. 5(e), the transverse optical force F_x exerted on a polystyrene sphere, due to the excited asymmetrical SPhPs, gradually increases with the sphere's radius when the electric dipole source is circularly

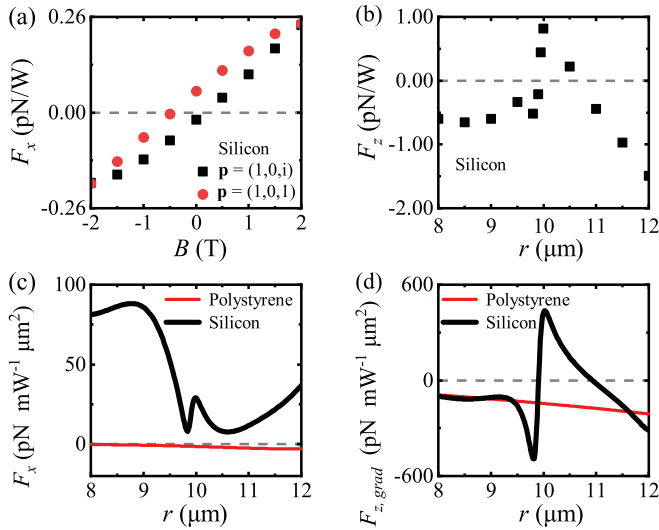


FIG. 6. (a) Transverse optical forces exerted on a silicon sphere (with a permittivity of 12.25 and a radius of $10 \mu\text{m}$) located at $(x/\lambda, y/\lambda, z/\lambda) = (0, 2.7, 0.3)$ vs the applied magnetic field. (b) The z component of the optical force exerted on a silicon sphere located at $(x/\lambda, y/\lambda) = (0, 2.7)$ vs the spheres' radius. The dipole source, with a radiation wavelength of $50 \mu\text{m}$, is positioned at $z_0 = 0.5 \mu\text{m}$ above the substrate surface in (a) and (b). (c) Transverse optical forces exerted on either a silicon or polystyrene sphere vs the sphere's radius. (d) The z component of optical forces (pure gradient force) exerted on either a silicon or polystyrene sphere vs the sphere's radius. The incident light in (c) and (d) is a linearly diagonally polarized evanescent wave, which propagates along the y direction and decays in the $z > 0$ half space. The evanescent wave's exponential decay rate is set to $0.6k$, with a wavelength of $50 \mu\text{m}$, and the intensity is $1 \text{ mW}/\mu\text{m}^2$ at the $z = 0$ plane. Both the silicon sphere and the polystyrene sphere in (b), (c), and (d) are situated $5 \mu\text{m}$ away from the $z = 0$ plane at their base.

polarized. However, in the case of a linearly diagonally polarized electric dipole source, the transverse optical force on the sphere changes sign with increasing radius. This change is a consequence of the competition between two mechanisms under varying radius conditions: the source's propagating component's asymmetry, and the total optical field's complex Poynting vector's imaginary part. Despite the increase of transverse force, manipulating the polystyrene sphere remains a challenge. This difficulty arises because the force F_z on the polystyrene sphere also increase and is less than zero [see Fig. 5(f)], resulting in significant adhesion forces that impede the sphere's manipulation.

We then select particle materials with a distinct permittivity difference from the background, such as a silicon sphere, to calculate the transverse optical force, as shown in Fig. 6(a). In the case of a circularly polarized or a linearly diagonally polarized electric dipole source, the transverse optical force can increase to several hundred fN/W, compared to the polystyrene sphere scenario [see Figs. 4(d) and 4(e)]. Additionally, the direction of the transverse optical force is also tunable. Interestingly, the transverse optical force behavior of the silicon sphere in Fig. 6(a) differs from that of polystyrene [see Figs. 4(d) and 4(e)]. To understand this, we calculate the transverse optical forces on the sphere in a linearly diagonally

polarized evanescent wave. In this scenario, the transverse optical force entirely results from the imaginary part of the Poynting vector of the incident evanescent wave [10,12]. As illustrated in Fig. 6(c), the resulting transverse optical forces on silicon and polystyrene spheres are exactly opposite due to their different electromagnetic properties. Moreover, Fig. 6(d) reveals that, for a particle radius of $10 \mu\text{m}$ in such a wave, the optical forces (pure gradient forces) on silicon and polystyrene spheres in the decay direction are also opposite. The polystyrene sphere is drawn towards the region of highest intensity by the gradient force, whereas the gradient force on the silicon sphere pushes it away from this area. Due to similar reasons, in the optical field of an electric dipole source near a doped InSb substrate, the transverse optical forces exerted on silicon and polystyrene spheres exhibit different behaviors. However, not all silicon sphere sizes are suitable for optical manipulation. As Fig. 6(b) illustrates, not all silicon sphere radii yield a positive F_z . By selecting an appropriately sized silicon sphere, the F_z it obtains is positive, opposing the gravitational force direction. This allows the silicon sphere to keep a certain distance from the substrate surface, effectively reducing the van der Waals force.

V. CONCLUSION

We have studied the transverse optical force on an achiral particle in an electric dipole source field near a doped InSb substrate. Since we specifically examine the transverse force on a particle located on the y axis, we employ two types of electric dipole sources polarized in the xz plane for near-field manipulation. These sources are a circularly polarized electric dipole source [$\mathbf{p} = (1, 0, i)$] and a linearly diagonally polarized electric dipole source [$\mathbf{p} = (1, 0, 1)$]. Our findings show that the transverse force arises from the symmetry breaking of the optical field along the x axis and is the outcome of a competition between four mechanisms. These mechanisms include the asymmetry of the source's propagating component, the asymmetric excitation of SPhPs from the source's evanescent component, the complex Poynting vector's imaginary part of the total optical field, and the nonreciprocal dispersion of SPhPs due to the applied magnetic field. For a circularly polarized electric dipole source, the transverse force results from the competition between the second and fourth mechanisms, while in the case of a linearly diagonally polarized electric dipole source, it results from the first, third, and fourth mechanisms. More importantly, the magnetic field can effectively tune the magnitude and sign of the transverse optical forces in both dipole source cases. Furthermore, by choosing an isotropic sphere with a significant permittivity difference from the background, the transverse optical force can be enhanced. Additionally, by selecting suitable radii for this sphere, adhesion forces can be reduced. Our paper introduces means to generate and control transverse optical forces.

ACKNOWLEDGMENTS

We gratefully acknowledge support from National Natural Science Foundation of China (Grants No. 12174231 and No. 12074230) and from the Fundamental Research Program of Shanxi Province through Project No. 202103021222001,

a Fund for Shanxi 1331 project, Research Project supported by Shanxi Scholarship Council of China, Program of

Education and Teaching Reform in Shanxi Province (Grant No. J20230003).

- [1] S. B. Wang and C. T. Chan, *Nat. Commun.* **5**, 3307 (2014).
- [2] M. H. Alizadeh and B. M. Reinhard, *ACS Photonics* **2**, 942 (2015).
- [3] Y. Shi, T. Zhu, T. Zhang, A. Mazzulla, D. P. Tsai, W. Ding, A. Q. Liu, G. Cipparrone, J. J. Sáenz, and C. Wei Qiu, *Light: Sci. Appl.* **9**, 62 (2020).
- [4] Y. Y. Tanaka, P. Albella, M. Rahmani, V. Giannini, S. A. Maier, and T. Shimura, *Sci. Adv.* **6**, eabc3726 (2020).
- [5] F. Nan, F. J. Rodríguez-Fortuño, S. Yan, J. J. Kingsley-Smith, J. Ng, B. Yao, Z. Yan, and X. Xu, *Nat. Commun.* **14**, 6361 (2023).
- [6] H. Chen, H. Zheng, W. Lu, S. Liu, J. Ng, and Z. Lin, *Phys. Rev. Lett.* **125**, 073901 (2020).
- [7] S. V. Sukhov, V. Kajorndejnukul, R. R. Naraghi, and A. Dogariu, *Nat. Photonics* **9**, 809 (2015).
- [8] D. T. O'Connor, P. Ginzburg, F. J. Rodríguez-Fortuño, G. A. Wurtz, and A. V. Zayats, *Nat. Commun.* **5**, 5327 (2014).
- [9] Y. Fu, Y. Zhang, C. Min, K. Fu, and X. Yuan, *Opt. Express* **28**, 13116 (2020).
- [10] K. Y. Bliokh, A. Y. Bekshaev, and F. Nori, *Nat. Commun.* **5**, 3300 (2014).
- [11] M. H. Alizadeh and B. M. Reinhard, *ACS Photonics* **2**, 1780 (2015).
- [12] X. Yu, Y. Li, B. Xu, X. Wang, L. Zhang, J. Chen, Z. Lin, and C. T. Chan, *Laser Photonics Rev.* **17**, 2300212 (2023).
- [13] A. A. Zharov, A. A. Zharov, I. V. Shadrivov, and N. A. Zharova, *Phys. Rev. A* **94**, 063845 (2016).
- [14] Y. Shi, T. Zhu, J. Liu, D. P. Tsai, H. Zhang, S. Wang, C. T. Chan, P. C. Wu, A. V. Zayats, F. Nori, and A. Q. Liu, *Sci. Adv.* **8**, eabn2291 (2022).
- [15] H. Magallanes and E. Brasselet, *Nat. Photonics* **12**, 461 (2018).
- [16] T. Zhang, M. R. C. Mahdy, Y. Liu, J. H. Teng, C. T. Lim, Z. Ping Wang, and C. Wei Qiu, *ACS Nano* **11**, 4292 (2017).
- [17] A. Y. Bekshaev, K. Y. Bliokh, and F. Nori, *Opt. Express* **21**, 7082 (2013).
- [18] M. Nieto-Vesperinas and J. J. Saenz, *Opt. Lett.* **35**, 4078 (2010).
- [19] E. A. Guzmán and A. V. Arzola, *J. Opt. Soc. Am. B* **39**, 1233 (2022).
- [20] J. S. Eismann, L. H. Nicholls, D. J. Roth, M. A. Alonso, M. A. Alonso, P. Banzer, F. J. Rodríguez-Fortuño, A. V. Zayats, F. Nori, and K. Y. Bliokh, *Nat. Photonics* **15**, 156 (2021).
- [21] T. V. Mechelen and Z. Jacob, *Optica* **3**, 118 (2016).
- [22] F. Kalthor, T. Thundat, and Z. Jacob, *Appl. Phys. Lett.* **108**, 061102 (2016).
- [23] X. Han and C. Sun, *Appl. Sci.* **9**, 3596 (2019).
- [24] Y. Zhang, C. Min, X. Dou, X. you Wang, H. P. Urbach, M. G. Somekh, and X. Yuan, *Light: Sci. Appl.* **10**, 475 (2021).
- [25] L. Novotny and B. Hecht, *Principles of Nano-Optics*, 2nd ed. (Cambridge University, New York, 2012).
- [26] E. D. Palik, R. Kaplan, R. W. Gammon, H. Kaplan, R. F. Wallis, and J. J. Quinn, *Phys. Rev. B* **13**, 2497 (1976).
- [27] S. Edelstein, A. Garcia-Martin, P. A. Serena, and M. I. Marqués, *Opt. Express* **30**, 28668 (2022).
- [28] G. Tang, L. Zhang, Y. Zhang, J. Chen, and C. T. Chan, *Phys. Rev. Lett.* **127**, 247401 (2021).
- [29] A. Archambault, T. V. Teperik, F. Marquier, and J. J. Greffet, *Phys. Rev. B* **79**, 195414 (2009).
- [30] L. Novotny, *J. Opt. Soc. Am. A* **14**, 91 (1997).
- [31] J. Gargiulo, T. Brick, I. L. Violi, F. C. Herrera, T. Shibanuma, P. Albella, F. G. Requejo, E. Cortés, S. A. Maier, and F. D. Stefani, *Nano Lett.* **17**, 5747 (2017).
- [32] Y. Cheng, K. A. Oyesina, B. Xue, D. Lei, A. M. H. Wong, and S. Wang, *Proc. Natl. Acad. Sci. USA* **120**, e2301620120 (2023).
- [33] M. F. Picardi, C. P. T. McPolin, J. J. Kingsley-Smith, X. Zhang, S. Xiao, F. J. Rodríguez-Fortuño, and A. V. Zayats, *Appl. Phys. Rev.* **9**, 021410 (2022).
- [34] B. Hecht, H. Bielefeldt, L. Novotny, Y. Inouye, and D. W. Pohl, *Phys. Rev. Lett.* **77**, 1889 (1996).
- [35] E. Betzig, J. K. Trautman, T. D. Harris, J. S. Weiner, and R. L. Kostelak, *Science* **251**, 1468 (1991).
- [36] F. J. Rodríguez-Fortuño, N. Engheta, A. Martínez, and A. V. Zayats, *Nat. Commun.* **6**, 8799 (2015).
- [37] M. F. Picardi, A. Manjavacas, A. V. Zayats, and F. J. Rodríguez-Fortuño, *Phys. Rev. B* **95**, 245416 (2017).
- [38] H. Kano, S. Mizuguchi, and S. Kawata, *J. Opt. Soc. Am. B* **15**, 1381 (1998).
- [39] N. Rotenberg, M. Spasenović, T. L. Krijger, B. le Feber, F. J. García de Abajo, and L. Kuipers, *Phys. Rev. Lett.* **108**, 127402 (2012).
- [40] F. J. Rodríguez-Fortuño, G. Marino, P. Ginzburg, D. O'Connor, A. Martínez, G. A. Wurtz, and A. V. Zayats, *Science* **340**, 328 (2013).
- [41] M. F. Picardi, A. V. Zayats, and F. J. Rodríguez-Fortuño, *Laser Photonics Rev.* **13**, 1900250 (2019).
- [42] J. P. Balthasar Mueller and F. Capasso, *Phys. Rev. B* **88**, 121410(R) (2013).
- [43] Y. Zhong, X. Lin, J. Jiang, Y. Yang, G.-G. Liu, H. Xue, T. Low, H. Chen, and B. Zhang, *Light: Sci. Appl.* **15**, 2000388 (2021).
- [44] A. A. Zharov, A. A. Zharov, and N. A. Zharova, *J. Exp. Theor. Phys.* **123**, 17 (2016).
- [45] X. G. Xu, B. G. Ghamsari, J. Jiang, L. Gilburd, G. O. Andreev, C. Zhi, Y. Bando, D. V. Golberg, P. Berini, and G. C. Walker, *Nat. Commun.* **5**, 4782 (2014).
- [46] C. Khandekar, S. Buddhiraju, P. R. Wilkinson, J. K. Gimzewski, A. W. Rodriguez, C. Chase, and S. Fan, *Phys. Rev. B* **104**, 245433 (2021).
- [47] S. Buddhiraju, Y. Shi, A. Song, C. Wojcik, M. Minkov, I. A. Williamson, A. Dutt, and S. Fan, *Nat. Commun.* **11**, 674 (2020).
- [48] S. Pakniyat, A. M. Holmes, G. W. Hanson, S. A. H. Gangaraj, M. Antezza, M. G. Silveirinha, S. Jam, and F. Monticone, *IEEE Trans. Antennas Propag.* **68**, 3718 (2019).
- [49] K. J. Shayegan, B. Zhao, Y. Kim, S. Fan, and H. A. Atwater, *Sci. Adv.* **8**, eabm4308 (2022).
- [50] J. A. Girón-Sedas, J. J. Kingsley-Smith, and F. J. Rodríguez-Fortuño, *Phys. Rev. B* **100**, 075419 (2019).

- [51] D. J. Griffiths, *Am. J. Phys.* **80**, 7 (2012).
- [52] X. Li, J. Chen, Z. Lin, and J. Ng, *Sci. Adv.* **5**, eaau7814 (2019).
- [53] N. K. Paul and J. S. Gomez-Diaz, *Phys. Rev. B* **107**, 035417 (2023).
- [54] J. J. Brion, R. F. Wallis, A. Hartstein, and E. Burstein, *Phys. Rev. Lett.* **28**, 1455 (1972).
- [55] A. Ott and S.-A. Biehs, *Phys. Rev. B* **101**, 155428 (2020).
- [56] K. Shastri, M. I. Abdelrahman, and F. Monticone, *Photonics* **8**, 133 (2021).